Simulation of an industrial semibatch nylon 6 reactor: optimal parameter estimation

Rajesh M. Wajge, S. Sreenivasa Rao and Santosh K. Gupta*
Department of Chemical Engineering, Indian Institute of Technology, Kanpur 208 016, India
(Received 9 July 1993)

This work presents a comprehensive computer simulation study for the hydrolytic polymerization of ε-caprolactam with the vaporization of both water and ε-caprolactam in an industrial semibatch reactor. It incorporates various correlations for heat and mass transfer, desorption from the free surface as well as bubbly desorption, and the build-up of pressure in the reactor. The solution of the mass and energy balance equations is carried out using Gear's algorithm. Optimal values of five parameters are obtained using the Box complex technique with industrial data for a feed-water concentration of 3.45 mass%. Simulation results are then obtained for two other feed-water concentrations using these curve-fitted parameter values. Excellent agreement is obtained with the corresponding industrial data. The activity coefficients of the monomer and water have been correlated with monomer conversion in this study. This eliminates infeasible solutions under certain conditions. The sensitivity of the model results to changes in the values of several parameters is also studied. The model developed can be used to optimize the performance of the reactor.

(Keywords: computer simulation; semibatch reactor; nylon 6)

INTRODUCTION

In recent years, numerical simulation and optimization of chemical reactors in general, and polymerization reactors in particular, have become increasingly popular as a means of understanding the behaviour of reactors and improving their performance. The commercial importance of nylon 6 has stimulated a considerable amount of research directed towards the modelling and simulation of its polymerization through the hydrolytic route in various industrial reactors. These have been reviewed by several workers[1–4].

The present work focuses on the simulation of an industrial semibatch nylon 6 reactor with vaporization of both ε-caprolactam (monomer) and water, being operated in a plant in India. Computer simulations based on the mathematical modelling of the polymerization process in this reactor are of paramount importance for quality control, process control and operational optimization of the existing plant, as well as in the design of similar new plants. This study predicts several molecular characteristics of the polymer manufactured and relates them to parameters characterizing the reactor. These molecular characteristics include molecular weight distribution (*MWD*), number average molecular weight (M_n, or degree of polymerization, *DP* or μ_n), polydispersity index (*PDI*), weight average molecular weight (M_w), per cent water extractables, end-group concentrations ([$-NH_2$] and [-COOH]), cyclic dimer concentration and monomer conversion. The reactor characteristics include heat and mass transfer parameters, kinetics of the reactions, feed-water concentration and jacket fluid temperature.

The industrial reactor configuration modelled is shown schematically in *Figure 1*. The semibatch polymerization reactor (autoclave) is a jacketed vessel having a low-speed anchor or ribbon agitator generally used for mixing fluids with high viscosities. A charge consisting of ε-caprolactam (C_1), water (W) and other additives (such as acetic acid, TiO_2, etc.) is fed to the reactor, which is kept under a nitrogen atmosphere. The reaction mass is heated by condensing vapours in the jacket. A pressure history is maintained in the reactor using a control valve through which vapours can be released as desired. The operation of the reactor can be described in terms of five stages or 'regions'. In stage 1, the charge is heated gradually to 250–270°C. During this time, vaporization of some water and ε-caprolactam takes place, gradually building up the pressure in the reactor (the valve is kept closed). When the pressure in the reactor reaches a certain value, P_{set}, the control valve opens and releases the vapours into a condensor line, in such a manner that the pressure is maintained at P_{set} for a specified period (this is referred to as stage 2). In the third, fourth and fifth stages, the control valve is operated so that the pressure drops linearly (at three different rates), finally reaching a pressure slightly above atmospheric at the end of the fifth stage.

This industrial reactor has been modelled by our group previously[5,6], but the model developed is unsuitable for optimization purposes owing to the presence of discontinuities in the equations for the activity coefficients of ε-caprolactam and water. Moreover, the equations used earlier for the activity coefficients lead to infeasible solutions when the reactor is simulated under some conditions that differ from those reported previously. In this study, we develop better correlations for the activity

* To whom correspondence should be addressed

0032-3861/94/17/3722–13

coefficients which do not suffer from this drawback, and obtain optimal values of the parameters in these correlations.

FORMULATION

The reaction mechanism comprises three major reactions, namely ring opening of ε-caprolactam (C_1) (by water (W) to form aminocaproic acid (S_1)), polycondensation and polyaddition. In addition, there are several important side reactions. Among these are the formation of cyclic oligomers, desamination and peroxidation of ε-caprolactam. The most important side reactions are those associated with cyclic oligomers, since their presence in the product causes problems in its processing (e.g. in spinning and moulding). The kinetic scheme considered in this work is shown in *Table 1*. This includes the three main reactions and the reactions associated with the cyclic dimer (C_2). The other cyclization reactions are omitted, since precise values of the parameters characterizing their rate constants are not yet available in the open literature. It is well known that the cyclic dimer constitutes the major share of the total cyclic oligomers and so the former can be used as a good first-order approximation of the total cyclics present.

The reactions are known to be autocatalytic. The rate constants are functions of the concentration of the acid end group. The apparent rate constants are of the form: $k_i = k_i^o + k_i^c[\text{–COOH}]$, with Arrhenius forms being used for k_i^o and k_i^c. All the reactions in *Table 1* are reversible. The temperature dependence of the equilibrium constants, K_i, are given by standard thermodynamic relations. The rate and equilibrium constants for the reactions of *Table 1* are given in *Table 2*. These are based on results from a series of experiments carried out by Tai *et al.*[2,7–12] using a non-linear regression analysis.

The present model of the semibatch reactor considers the following aspects: heat transfer from the jacket fluid to the reaction mass, vaporization of water and ε-caprolactam from the reaction mass, build-up of pressure and maintenance of a pressure history above

Table 1 Kinetic scheme for nylon 6 polymerization

1. Ring opening

$$C_1 + W \underset{k_1' = k_1/K_1}{\overset{k_1}{\rightleftharpoons}} S_1$$

2. Polycondensation

$$S_n + S_m \underset{k_2' = k_2/K_2}{\overset{k_2}{\rightleftharpoons}} S_{n+m} + W$$

3. Polyaddition

$$S_n + C_1 \underset{k_3' = k_3/K_3}{\overset{k_3}{\rightleftharpoons}} S_{n+1}$$

4. Ring opening of cyclic dimer

$$C_2 + W \underset{k_4' = k_4/K_4}{\overset{k_4}{\rightleftharpoons}} S_2$$

5. Polyaddition of cyclic dimer

$$S_n + C_2 \underset{k_5' = k_5/K_5}{\overset{k_5}{\rightleftharpoons}} S_{n+2}$$

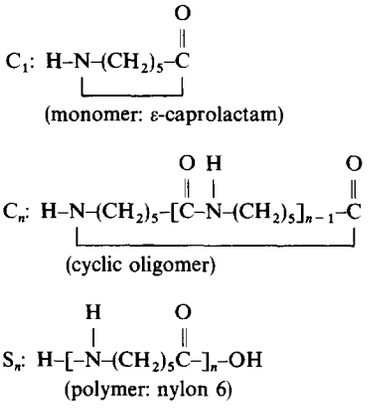

W: H_2O

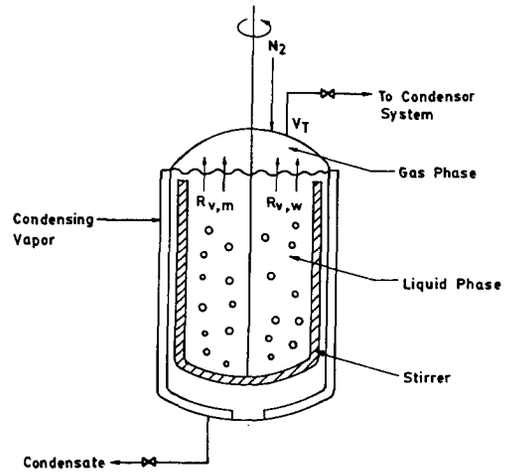

Figure 1 Schematic representation of the industrial semibatch nylon 6 reactor

Table 2 Rate and equilibrium constants

$$k_1 = k_i^o + k_i^c[\text{–COOH}] = A_i^o \exp(-E_i^o/RT) + A_i^c \exp(-E_i^c/RT)[\text{–COOH}] = k_i^o + k_i^c \sum_{n=1}^{\infty} ([S_n])$$

$$K_i = \exp[(\Delta S_i - \Delta H_i/T)/R], \qquad i = 1, 2, \ldots, 5$$

i	A_i^o (kg mol^{-1} h^{-1})	E_i^o (J mol^{-1})	A_i^c (kg^2 mol^{-2} h^{-1})	E_i^c (J mol^{-1})	ΔH_i (J mol^{-1})	ΔS_i (J mol^{-1} K^{-1})
1	5.9874×10^5	8.3198×10^4	4.3075×10^7	7.8703×10^4	8.0268×10^3	-3.2997×10^1
2	1.8942×10^{10}	9.7389×10^4	1.2114×10^{10}	8.6504×10^4	-2.4883×10^4	3.9496×10^0
3	2.8558×10^9	9.5606×10^4	1.6377×10^{10}	8.4148×10^4	-1.6923×10^4	-2.9068×10^1
4	8.5778×10^{11}	1.7577×10^5	2.3307×10^{12}	1.5652×10^5	-4.0176×10^4	-6.0766×10^1
5	2.5701×10^8	8.9141×10^4	3.0110×10^9	8.5374×10^4	-1.3263×10^4	2.4384×10^0

Table 3 Mass and energy balance equations[6,15]

$$\frac{d[C_1]}{dt} = -k_1[C_1][W] + k'_1[S_1] - k_3[C_1]\mu_o + k'_3(\mu_o - [S_1]) - R_{vm}/F + [C_1]\frac{0.113R_{vm} + 0.018R_{vw}}{F}$$

$$\frac{d[S_1]}{dt} = k_1[C_1][W] - k'_1[S_1] - 2k_2[S_1]\mu_o + 2k'_2[W](\mu_o - [S_1]) - k_3[S_1][C_1] + k'_3[S_2] - k_5[S_1][C_2] + k'_5[S_3] + [S_1]\frac{0.113R_{vm} + 0.018R_{vw}}{F}$$

$$\frac{d\mu_0}{dt} = k_1[C_1][W] - k'_1[S_1] - k_2\mu_o^2 + k'_2[W](\mu_1 - \mu_o) + k_4[W][C_2] - k'_4[S_2] + \mu_o\frac{0.113R_{vm} + 0.018R_{vw}}{F}$$

$$\frac{d\mu_1}{dt} = k_1[C_1](W] - k'_1[S_1] + k_3[C_1]\mu_o - k'_3(\mu_o - [S_1]) + 2k_5[C_2]\mu_o - 2k'_5(\mu_o - [S_1] - [S_2]) + 2k_4[W][C_2] - 2k'_4[S_2] + \mu_1\frac{0.113R_{vm} + 0.018R_{vw}}{F}$$

$$\frac{d\mu_2}{dt} = k_1[C_1][W] - k'_1[S_1] + 2k_2\mu_1^2 + \frac{1}{3}k'_2[W](\mu_1 - \mu_3) + k_3[C_1](\mu_o + 2\mu_1) + k'_3(\mu_o - 2\mu_1 + [S_1]) + 4k_5[C_2](\mu_o + \mu_1) + 4k'_5(\mu_o - \mu_1 + [S_2]) + 4k_4[W][C_2] - 4k'_4[S_2] + \mu_2\frac{0.113R_{vm} + 0.018R_{vw}}{F}$$

$$\frac{d[C_2]}{dt} = -k_4[C_2][W] + k'_4[S_2] - k_5[C_2]\mu_o + k'_5(\mu_o - [S_1] - [S_2]) + [C_2]\frac{0.113R_{vm} + 0.018R_{vw}}{F}$$

$$\frac{d[W]}{dt} = -k_1[C_1][W] + k'_1[S_1] + k_2\mu_o^2 - k'_2[W](\mu_1 - \mu_o) - k_4[C_2][W] + k'_4[S_2] - R_{vw}/F + [W]\frac{0.113R_{vm} + 0.018R_{vw}}{F}$$

$$\frac{dF}{dt} = -(0.113R_{vm} + 0.018R_{vw})$$

$$\frac{dT}{dt} = \left\{UA(T_j - T) + \frac{F}{1000}\sum_{i=1}^{5} r_i(-\Delta H_i) - [R_{vm}\lambda_m(T_r) + R_{vw}\lambda_w(T_r)] - [0.113R_{vm}C^v_{p,m} + 0.018R_{vw}C^v_{p,w}](T - T_r) + C^l_{p,mix}[0.113R_{vm} + 0.018R_{vw}](T - T_r)\right\} \times \{[C^l_{p,mix} + 2.0925 \times 10^{-3}(T - T_r)]F\}^{-1}$$

$$\frac{d[M^v]}{dt} = \frac{R_{vm}}{V_g} - \frac{V_T[M^v]}{V_g([M^v] + [W^v] + [N^v])}$$

$$\frac{d[W^v]}{dt} = \frac{R_{vw}}{V_g} - \frac{V_T[W^v]}{V_g([M^v] + [W^v] + [N^v])}$$

$$\frac{d[N^v]}{dt} = -\frac{V_T[N^v]}{V_g([M^v] + [W^v] + [N^v])}$$

$$\frac{d\zeta_1}{dt} = R_{vm}$$

$$\frac{d\zeta_2}{dt} = R_{vw}$$

$$\frac{d\zeta_3}{dt} = V_T$$

Closure conditions:

$$[S_3] = [S_2] = [S_1]$$

$$\mu_3 = \frac{\mu_2(2\mu_2\mu_0 - \mu_1^2)}{\mu_1\mu_0}$$

the liquid reaction mass in the reactor, change in the viscosity of the reaction mixture during polymerization and its affect on the heat and mass transfer rates, and the various reactions leading to the formation of the polymer and side products. Two types of vaporization take place and are accounted for in our model. The first is quiescent desorption from the free surface of the liquid near the top of the reactor, while the second is through bubbles formed in the liquid owing to the supersaturation of the liquid phase resulting from the rise in temperature.

Gupta *et al.*[5,6] have presented a preliminary model for this industrial semibatch reactor. They studied several vapour–liquid equilibrium correlations, and found that the best agreement with industrial data was obtained using correlations for the activity coefficients of the two volatiles (C_1 and W) based on experimental data of Giori and Hayes[13,14]. The rates of vaporization of water and ε-caprolactam were described in terms of appropriate mass transfer coefficients and equilibrium interfacial concentrations. The present model differs from the previous one in two ways: the energy balance equation and the equations for the activity coefficients for the two volatiles, monomer (m) and water (w), are different. The complete set of equations as well as the various correlations and other relevant equations[15–20] used in this study are presented in *Tables 3* and *4*. The variables used are defined in the Nomenclature. Details can be found in refs 6 and 15 and are not repeated here for the sake of brevity.

The energy balance equation used by Gupta *et al.*[6,15] was:

$$\frac{dT}{dt} = \frac{UA(T_j - T)}{C^l_{p,mix}} + \frac{F}{1000C^l_{p,mix}}\sum_{i=1}^{5} r_i(-\Delta H_i) - \frac{R_{vm}\lambda_m(T) + R_{vw}\lambda_w(T)}{FC^l_{p,mix}} + T\frac{0.113R_{vm} + 0.018R_{vw}}{F} \quad (1)$$

Table 4 Correlations and other equations used

Expression for V_T

Stage 1: $V_T = 0$

Stages 2–5: $V_T = R_{vm} + R_{vw} - \frac{V_g}{RT}\left(\frac{dP}{dt}\right) + V_g \frac{[M^v]+[W^v]+[N^v]}{T}\left(\frac{dT}{dt}\right)$

Rates of vaporization

$R_{vm} = F(k_{l,m}a)_f([C_1]-[C_1]^*_f) \qquad [C_1]^*_f = \frac{[W]+[C_1]}{\gamma_m P^{sat}_m}[M^v]RT$

$R_{vw} = F(k_{l,w}a)_f([W]-[W]^*_f) + F(k_{l,w}a)_b([W]-[W]^*_b)$

$[W]^*_f = \frac{[W]+[C_1]}{\gamma_w P^{sat}_w}[W^v]RT \qquad [W]^*_b = \frac{[C_1](P-\gamma_m P^{sat}_m)}{(\gamma_w P^{sat}_w - P)}$

Pressure

$P = \{[M^v]+[W^v]+[N^v]\}RT$

Equations for activity coefficients

$\text{monomer conversion} = 1.0 - \frac{F[C_1]}{F_o[C_1]_o - \zeta_1}$

$\gamma_m = \beta_{mo} + \frac{\beta_{mf}-\beta_{mo}}{0.95}(\text{monomer conversion})$

$\gamma_w = \beta_{wo} + \frac{\beta_{wf}-\beta_{wo}}{0.95}(\text{monomer conversion})$

Vapour pressure

$\ln[P^{sat}_m\ (\text{kPa})/101.3] = 13.0063 - \frac{7024.023}{T(\text{K})}$ (ref. 16)

$\ln[P^{sat}_w\ (\text{kPa})/101.3] = 11.6703 - \frac{3816.44}{T(\text{K})-46.13}$ (ref. 17)

Diffusion coefficients

$\mathscr{D}_w\ (\text{m}^2\ \text{h}^{-1}) = 3.6 \times 10^{-6}$

$\mathscr{D}_m\ (\text{m}^2\ \text{h}^{-1}) = 2.88 \times 10^{-8}$

Latent heats of vaporization

$T_r = 473.15$ K

$\lambda_w(T_r) = 34.2559\ \text{kJ mol}^{-1}$ (ref. 18)

$\lambda_m(T_r) = 51.0193\ \text{kJ mol}^{-1}$ (ref. 18)

$C^v_{p,m} = 1.6426\ \text{kJ kg}^{-1}\ \text{K}^{-1}$ (ref. 18)

$C^v_{p,w} = 1.9963\ \text{kJ kg}^{-1}\ \text{K}^{-1}$ (ref. 18)

Heat transfer coefficient

$h_i\ (\text{kJ h}^{-1}\ \text{m}^{-2}\ \text{K}^{-1}) = \frac{h_{ref}}{[\eta\ (\text{Pa s})]^{0.17}}$

$U = \frac{1}{\frac{1}{h_i} + \frac{\text{thickness (m)}}{k_{ss}}}$

Correlations from ref. 19 for mixture physical properties (liquid)

$C^l_{p,mix}\ (\text{kJ kg}^{-1}\ \text{K}^{-1}) = 2.0925 + 2.0925 \times 10^{-3}\ [T(\text{K}) - 273.15]$

$\rho\ (\text{kg m}^{-3}) = 1000\{1.1238 - 0.5663 \times 10^{-3}\ [T(\text{K}) - 273.15]\}$

$k\ (\text{kJ h}^{-1}\ \text{m}^{-1}\ \text{K}^{-1}) = 0.7558$

Correlations from ref. 20 for mass transfer coefficients

$N_{Re} = \frac{d_s^2 n \rho}{6\eta(\text{poise})}$

$N_{Sc,i} = \frac{360\eta(\text{poise})}{\rho \mathscr{D}_i}$

$\Omega_b \equiv \left(\frac{[C_1]}{[C_1]+[W]}\gamma_m P^{sat}_m + \frac{[W]}{[C_1]+[W]}\gamma_w P^{sat}_w\right)$

(i) Quiescent (q) desorption ($\Omega_b < P$)

$N_{Sh,i,q} = 0.322 N^{0.7}_{Re} N^{0.33}_{Sc,i} \qquad i = \text{m or w}$

$N_{Sh,i,q} = \frac{(k_{l,i})_{f,q} D_r}{\mathscr{D}_i}$

$a_{f,q} = \frac{(\pi/4)D_r^2}{(F/\rho)}$

$(k_{l,m}a)_f = (k_{l,m}a)_{f,q}$

$(k_{l,w}a)_f = (k_{l,w}a)_{f,q}$

$(k_{l,w}a)_b = 0$

(ii) Bubbly (b) desorption ($\Omega_b > P$)

$\sigma \equiv \frac{[W]-[W_b]^*}{[W_b]^*}$

$\sigma_c \equiv 1.81 N^{-0.25}_{Re}$

If $\sigma < \sigma_c$:

$(k_{l,w}a)_b\ (\text{h}^{-1}) = 6.77 \times 10^{-6} N^{0.5}_{Re} \sigma^{0.78} \times 3600$

$(k_{l,m}a)_f = (k_{l,m}a)_{f,q}$

$(k_{l,w}a)_f = (k_{l,w}a)_{f,q}$

If $\sigma > \sigma_c$:

$(k_{l,w}a)_b (\text{h}^{-1}) = 2.45 \times 10^{-6} N^{0.93}_{Re} \sigma^{2.5} \times 3600$

$\log_{10}\phi \equiv 522(\sigma - \sigma_c) N^{-0.81}_{Re}$

$(k_{l,m}a)_f = (k_{l,m}a)_{f,q}\phi$

$(k_{l,w}a)_f = (k_{l,w}a)_{f,q}\phi$

Viscosity correlation (neglecting effect of water)

$\eta_m(\text{cp}) = 2.7969 \times 10^{-4} \exp[3636.364/T(\text{K})] \qquad \text{for } T > 473.15\ \text{K}$

$[\eta]\left(\frac{100\ \text{kg mixture}}{\text{kg polymer}}\right) \equiv \lim_{c\to 0}\frac{\eta_{sp}}{c} \equiv \lim_{c\to 0}\frac{\eta-\eta_m}{\eta_m}\frac{1}{c} = \left[-\frac{1875.0}{T(\text{K})} + 4.678\right]\left(\frac{M_n}{5424}\right)^{0.75}$

$M_n = 113\ \mu_1/\mu_o \qquad M_w = 113\ \mu_2/\mu_1$

$c\ (\text{kg polymer}/100\ \text{kg mixture}) = 11.3\ \mu_1$

For $c < 21.0/[\eta]$

$\frac{\eta_{sp}}{c[\eta]} = 1.0 - 0.3102c[\eta] + 0.0575(c[\eta])^2 - 0.525 \times 10^{-2}(c[\eta])^3 + 0.2305 \times 10^{-3}(c[\eta])^4 - 0.3663 \times 10^{-5}(c[\eta])^5$

For $c > 21.0/[\eta]$

$\log_{10}\eta\ (\text{poise}) = 5\log_{10}(C'_s M^{0.68}_w) - 12.3097$

for $C'_s M^{0.68}_w > 315$ and $M_w > 5000$

else

$\log_{10}\eta\ (\text{poise}) = \log_{10}(C'_s M_w) - 3.503$

where $C'_s\ (\text{g polymer/cm}^3\ \text{mixture}) = 11.3 \times 10^{-5}\rho\mu_1$

This is replaced by the following, more exact equation for the energy balance (for the liquid phase) in this study:

$$\frac{dT}{dt}=\left\{UA(T_j-T)+\frac{F}{1000}\sum_{i=1}^{5}r_i(-\Delta H_i)\right.$$
$$-[R_{vm}\lambda_m(T_r)+R_{vw}\lambda_w(T_r)]$$
$$-[0.113R_{vm}C^v_{p,m}+0.018R_{vw}C^v_{p,w}](T-T_r)$$
$$\left.+C^l_{p,mix}[0.113R_{vm}+0.018R_{vw}](T-T_r)\right\}$$
$$\times\{[C^l_{p,mix}+2.0925\times10^{-3}(T-T_r)]F\}^{-1} \quad (2)$$

Terms accounting for the temperature dependence of the latent heat of vaporization of monomer are incorporated in equation (2). Also, the specific heats of these two components in the vapour phase have been distinguished in equation (2).

The equations for the activity coefficients, γ_m and γ_w, for the monomer and water, respectively, used in our previous work[6,15] were:

For monomer conversions $>50\%$

$$\gamma_m=0.25$$
$$\gamma_w=0.135+0.9095x_w-2.842x_w^2+3.062x_w^3$$
$$x_w=\frac{[W]_i^*}{[W]_i^*+[C_1]_i^*+\mu_{0,i}^*+[C_2]_i^*}\approx\frac{[W]}{[W]+[C_1]}$$

For monomer conversions $<50\%$

$$\gamma_m=0.95$$
$$\gamma_w=0.60 \quad (3)$$

In this study the following equations have been used, which correlate the activity coefficients as simple, linear functions of the monomer conversion:

$$\gamma_m=\beta_{mo}+\frac{\beta_{mf}-\beta_{mo}}{0.95}(\text{monomer conversion})$$
$$\gamma_w=\beta_{wo}+\frac{\beta_{wf}-\beta_{wo}}{0.95}(\text{monomer conversion}) \quad (4)$$

where

$$\text{monomer conversion}\equiv1.0-\frac{F[C_1]}{F_o[C_1]_o-\zeta_1} \quad (5)$$

and β_{mo}, β_{mf}, β_{wo} and β_{wf} are four of the five constants to be obtained by curve-fitting industrial data. The linear variation of the activity coefficients with monomer conversion was selected after our initial attempts at fitting the industrial data using constant values of γ_m and γ_w failed.

Use of equation (4) offers two advantages. First, it does not involve a mathematical discontinuity at a monomer conversion of 0.5, in contrast to equation (3). This avoids the occurrence of sudden changes in the interfacial concentrations of monomer and water, and prevents the gradient of the concentration of monomer (at the bubble surface) from becoming negative. Such a numerical aberration associated with the use of equation (3) creates problems when simulating reactor operation under certain conditions not studied earlier[6]. Use of continuous equations for the two activity coefficients is expected to be of help in future work on the optimization of these reactors. The second advantage associated with the use of equation (4) stems from the fact that the correlating variable is monomer conversion. The mole fraction of water, x_w (in equation (3)), increases with time at the beginning. At later stages of polymerization (when the reaction mass contains a considerable mass of polymer), x_w decreases with time. The monomer conversion (in equation (4)), however, varies unimodally, and so is preferred as a correlating variable for the activity coefficients. Obviously, a more fundamental correlation relating γ_m and γ_w to the individual concentrations in the liquid and/or vapour phases would be better, but is not possible at the present stage owing to lack of sufficient vapour–liquid equilibrium data on model non-reacting systems of ε-caprolactam, water and nylon 6. Adaptations of the Flory–Huggins theory for the activity coefficients were tried, but they led to much lower pressures than encountered in the industrial reactor.

The equations in *Tables 3* and *4* form a complete set of equations (ordinary differential equations–initial value problem, ODE–IVP) and can be integrated for the given feed conditions. The numerical technique used to solve such sets of equations is Gear's algorithm. The NAG library routine D02EJF, which has a built-in step size control algorithm and is particularly useful for stiff systems, was used (with a tolerance, TOL, of 10^{-6}) for this purpose on an HP 9000/850S computer system.

Several checks were made on our computer program to ensure that it was free of errors. Simulations under isothermal, non-vaporizing conditions were carried out by setting $dT/dt=0$ in the program and using $k_{l,m}$ and $k_{l,w}$ as 0. The feed conditions used were:

$$[C_1]_o=8.8 \text{ mol kg}^{-1}$$
$$[W]_o=0.16 \text{ mol kg}^{-1} \quad (6)$$

with temperatures of 230, 240, 250 and 270°C. The results were found to be in complete agreement with those of Ray and Gupta[21], thus confirming the correctness of the several mass balance equations as well as the logic of the program. Similarly, adiabatic (and non-vaporizing) operation was simulated by setting the overall heat transfer coefficient, U, as zero. The results were found to match those of Pal and Gupta[22]. This further confirmed the correctness of the simulation program, including the energy balance equation.

The simulation program was then combined with a non-linear parameter-estimation program to obtain the best-fit values of five parameters, β_{mo}, β_{mf}, β_{wo}, β_{wf} and the heat transfer parameter, h_{ref}, used in the following equation (see *Table 4*) for the inside film heat transfer coefficient:

$$h_i(\text{kJ h}^{-1}\text{ m}^{-2}\text{ K}^{-1})=h_{ref}/[\eta(\text{Pa s})]^{0.17} \quad (7)$$

The Box complex method was used for this purpose. Some preliminary results show that the industrial data available to us on temperature, pressure and the number average chain length are quite sensitive to these five parameters. All other parameters and correlations are used as obtained from the literature (not necessarily on nylon 6 systems).

The Box complex procedure obtains values of the parameters, $p_1, p_2, \ldots, p_q$, which minimize some objective function, $E(p_1, p_2, \ldots, p_q)$, using a patterned-search technique. The objective function is chosen as a weighted sum of square errors between the values predicted by the

model and the industrial data:

$$E(\boldsymbol{p}) = E(p_1, p_2, \ldots, p_q) = w_1 \sum_{i=1}^{N_T} \left(\frac{\theta_{i,\text{expt}} - \theta_{i,\text{theor}}}{\theta_{i,\text{expt}}} \right)^2 + w_2 \sum_{i=1}^{N_P} \left(\frac{\Pi_{i,\text{expt}} - \Pi_{i,\text{theor}}}{\Pi_{i,\text{expt}}} \right)^2 + w_3 \left(\frac{\mu_{n,t_f,\text{expt}} - \mu_{n,t_f,\text{theor}}}{\mu_{n,t_f,\text{expt}}} \right)^2 \quad (8)$$

In equation (8), θ is the dimensionless temperature of the reaction mass (see Nomenclature), Π is the dimensionless pressure and μ_{n,t_f} is the value of the number average chain length of the polymer product (at $t = t_f$). N_T is the number of industrial data points available for θ, and N_P is the number of industrial data points available for Π. There is only a single value (at $t = t_f$) of μ_n available to us. w_1, w_2 and w_3 are the weightage factors.

RESULTS AND DISCUSSION

There is a considerable amount of inconsistency and scatter in the (relatively scarce) experimental data available on the activity coefficients of monomer and water for the ternary system ε-caprolactam–water–nylon 6. A detailed discussion of this has been presented in our earlier work[5,6,15]. *Figures 2* and *3* show the experimental results of Giori and Hayes[13,14] on the activity coefficients γ_m and γ_w. Some of these points (squares) represent results corresponding to the initial stages of polymerization where the mass fraction of polymer is close to zero. The remaining data points (circles) correspond to near-equilibrium ε-caprolactam–water–nylon 6 systems, where the mass fraction of the polymer is quite high (mole fraction of polymer ≈ 0.06). It is quite difficult to extract continuous functions for γ_m and γ_w over the entire range of monomer conversion from these diagrams. In fact, *Figures 2* and *3* can, at best, be used to infer limiting values of γ_m and γ_w at low and high monomer conversions. Correlations for γ_m and γ_w are thus ideal candidates for parameter estimation. In the absence of such information and as a first approximation, we have used a linear variation of γ_m and γ_w with monomer conversion, as given in equation (4).

Values of the five parameters, $\boldsymbol{p}[\equiv \beta_{mo}, \beta_{mf}, \beta_{wo}, \beta_{wf}, h_{ref}]$, have been obtained by curve-fitting one set of industrial data (temperature and pressure histories, and the final value of μ_n) available to us corresponding to the following conditions (referred to as the 'reference' run):

$$\begin{aligned} [C_1]_o &= 8.5442 \text{ mol kg}^{-1} & F &= * \text{ kg} \\ [W]_o &= 1.91667 \text{ mol kg}^{-1} \ (3.45 \text{ mass\%}) & [N^v]_o &= * \text{ mol m}^{-3} \\ T_o &= 90°C & D_r &= * \text{ m} \\ T_j &= 270°C & d_s &= * \text{ m} \\ P_o &= 101.3 \text{ kPa} & n &= * \text{ rev min}^{-1} \\ P_{set} &= * \text{ kPa} & V_g &= * \text{ m}^3 \\ t_f &= * \text{ h} \end{aligned} \quad (9)$$

Asterisks have been used to ensure confidentiality of the industrial data.

Figures 4 and *5* (curves a) show the model results for the dimensionless temperature and pressure defined by:

$$\theta \equiv \frac{T - T_o}{T_j - T_o}$$

$$\Pi \equiv \frac{P - P_o}{P_{set} - P_o} \quad (10)$$

as a function of the dimensionless time:

$$\tau \equiv \frac{t}{t_f} \quad (11)$$

for the reference conditions given in equation (9). The optimal parameter values used to generate those diagrams are given in *Table 5* (case a or reference values).

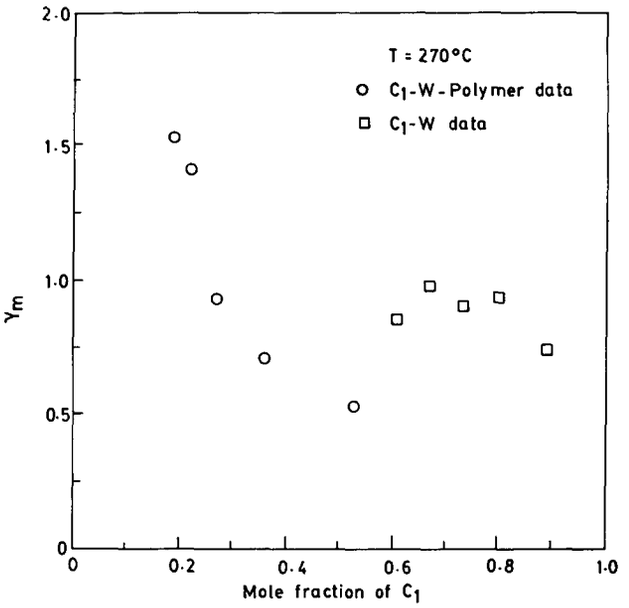

Figure 2 Vapour–liquid equilibrium data[13,14] for water–ε-caprolactam–nylon 6 system. ○, Data on the ternary system with polymer mole fraction of about 0.06; □, binary (C_1–W) data

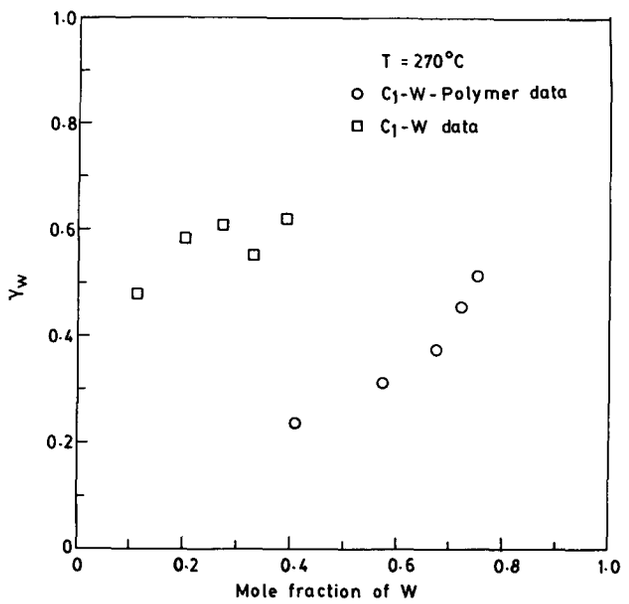

Figure 3 Vapour–liquid equilibrium data for water–ε-caprolactam–nylon 6 system[13,14]. Notation as in *Figure 2*

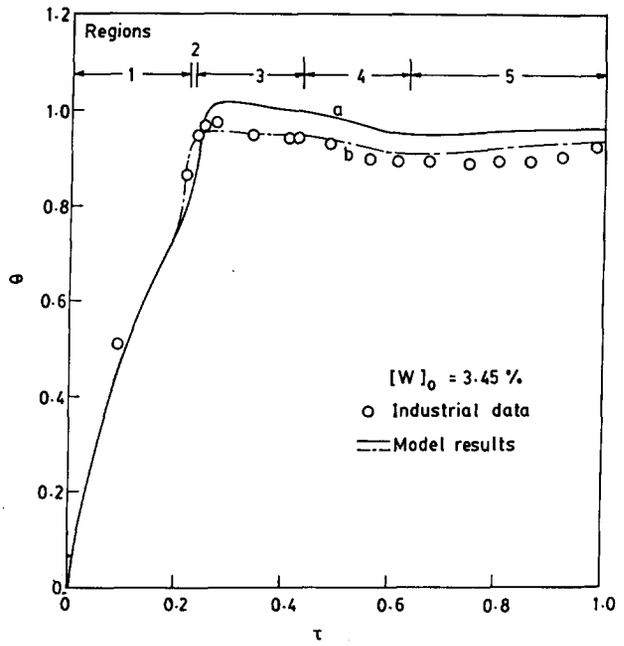

Figure 4 Variation of the dimensionless temperature, θ, with dimensionless time, τ, for $[W]_0 = 3.45$ mass%. ○, Industrial data; curves, model results using the best-fit values of the parameters as given in *Table 5* (Cases a (reference) and b)

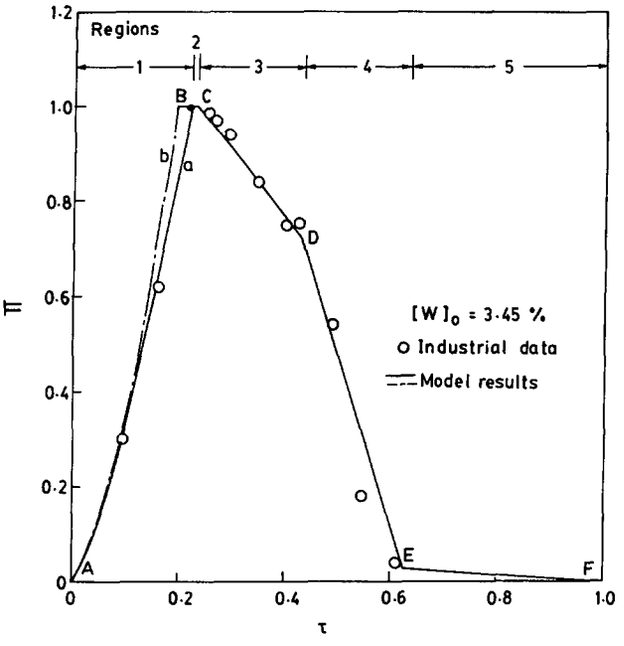

Figure 5 Variation of the dimensionless pressure, Π, with dimensionless tme, τ, for $[W]_0 = 3.45$ mass%. Notation as in *Figure 4*

The weightage factors w_1, w_2 and w_3 in equation (8) and the other parameters used in the Box complex program[23–25] are given in *Table 6*. The use of the parameter values given in *Table 5* along with the other equations in *Tables 3* and *4* does not give negative gradients of monomer concentration at the bubble surface (i.e. $[C_1]_f^* - [C_1] < 0$ is not encountered).

Figures 4 and *5* also show the industrial data. It may be mentioned that the straight line equations relating Π to τ in regions 3 (CD in *Figure 5*), 4 (DE) and 5 (EF) have been 'read-in' as inputs to the program (see *Table 7*). Similarly, the value of Π is maintained at 1.0 from the time the pressure, P, first reaches the value of P_{set} (point B) till a specified point, C, in *Figure 5*. Hence, it is appropriate to check the fit between industrial data on Π and model results only in region 1 (AB). N_P in equation (8) reflects this point.

Figures 4 and *5* (curves a) show fairly good agreement between industrial data and simulation results in region 1. The computed value of μ_n at $\tau = 1$ is 151.76, which agrees well with the industrial value of 152.5. It is seen that the predicted temperatures in regions 3–5 are slightly higher (the computed value of θ at $\tau = 1$ is 0.9633 compared to the industrial value of 0.925, corresponding to actual temperatures being higher by about 6–7°C), while pressures in region 1 are extremely close to the industrial values. The agreement in θ could be improved slightly by using a different set of values for $\boldsymbol{p}$, but this leads to a considerable worsening of the agreement in the values of μ_n at $\tau = 1$.

Table 5 Parameter values used for generating results

Parameter	Case a (reference)	Case b
E_3^s (J mol^{-1})	8.4148×10^4[a]	7.5733×10^4[a]
ΔH_3 (J mol^{-1})	-1.6923×10^4[a]	-1.5231×10^4[a]
$p_1 \equiv \beta_{mo}$	1.32789	1.3791
$p_2 \equiv \beta_{mf}$	0.156224	0.2
$p_3 \equiv \beta_{wo}$	1.33774	1.6331
$p_4 \equiv \beta_{wf}$	0.163764	0.184
$p_5 \equiv h_{ref}$	109.9952[b]	107.7931[b]

[a]These values are not obtained by the Box complex method
[b]Units defined by equation (7)

Table 6 Parameters used in Box complex[23–25] program

Weightage factors
$w_1 = 100.0$
$w_2 = 1.0$
$w_3 = 1.0$
$N = 5$
$\alpha = 1.3$
$\beta = 10^{-3}$
$\gamma = 5$
$\delta = 10^{-5}$
Random numbers generated using G05FAF of NAG library

Initial value of parameters, $\boldsymbol{p}$
$\boldsymbol{p} = [1.50, 0.18, 1.60, 0.14, 116.3974]^T$

Bounds on $\boldsymbol{p}$
$1.1 \leqslant \beta_{mo} \leqslant 1.7$
$0.14 \leqslant \beta_{mf} \leqslant 0.21$
$1.2 \leqslant \beta_{wo} \leqslant 1.8$
$0.14 \leqslant \beta_{wf} \leqslant 0.19$
$83.7 \leqslant h_{ref} \leqslant 141.5$

Table 7 Coordinates of points on the $\Pi(\tau)$ diagrams (*Figures 5, 10* and *12*)

	Coordinates (τ, Π) of points[a]		
$[W]_0$ (%)	C	D	E
2.52	(0.258, 1)	(0.4875, 0.5592)	(0.5906, 0.0377)
3.45	(0.2313, 1)	(0.4313, 0.7219)	(0.625, 0.0333)
4.43	(0.219, 1)	(0.3833, 0.9007)	(0.595, 0.02667)

[a]$\Pi_B = 1$. τ_B decided by vaporization. Point F is (1.0, 0.0067). Points C, D and E are common for cases a and b

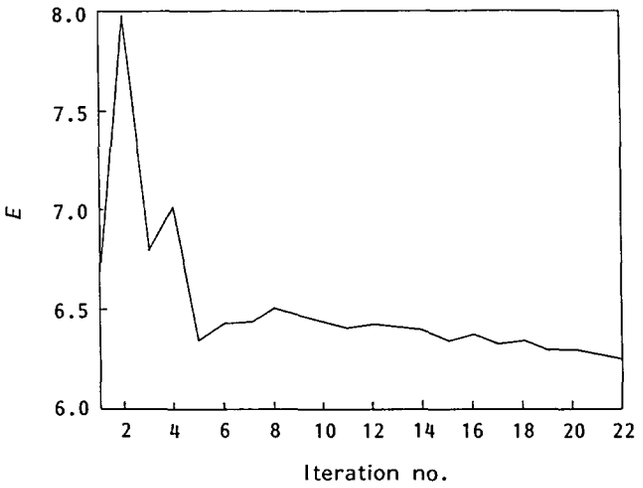

Figure 6 Results of the Box complex procedure for $[W]_0 = 3.45$ mass% (case a). Weighted sum of square errors, E, as a function of iteration number

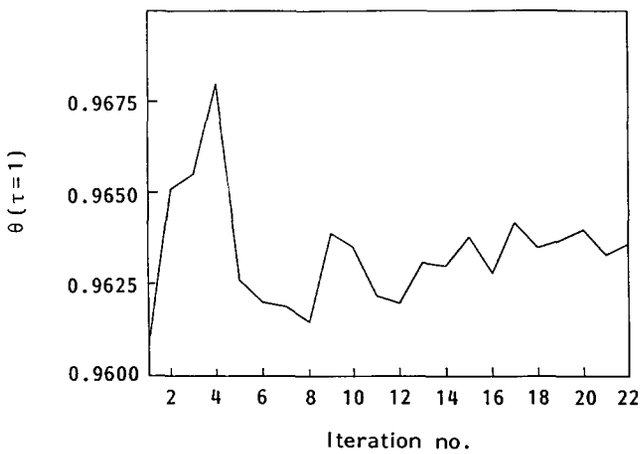

Figure 7 Variation of θ ($\tau = 1$) with iteration number for the case shown in *Figure 6*

Figures 6–8 show some intermediate results obtained from the Box complex procedure for this reference case. *Figure 6* shows how the error, E (equation (8)), varies with iteration number. In the early stages, the 'complex' having six vertices in the five-dimensional parameter space is large in size, and the error fluctuates significantly. Later, however, the 'complex' reduces in size, and the fluctuations in E are much less. In addition, the error decreases very slowly with iteration number. *Figure 7* shows how the value of θ at $\tau = 1$ also becomes relatively stable at high iterations. *Figure 8* shows how the value of μ_n of the product (μ_n at $\tau = 1$) approaches the experimental value of 152.5. It was decided to stop further computations and use the parameters corresponding to the 22nd iteration (these are given in *Table 5*, case a) as the final or 'best fit' values. The CPU time for the 22 iterations was 26 min on a supermini HP 9000/850S computer.

Figures 9–12 (curves a) show computed curves of $\theta(\tau)$ and $\Pi(\tau)$ for two more sets of industrial runs available to us, corresponding to $[W]_0 = 2.52$ mass% and 4.43 mass%. No curve-fitting or optimal parameter estimation was performed for these two cases. The model results in *Figures 9–12* (curves a) were obtained using values of the five parameters given in *Table 5*, case a (which were obtained by curve-fitting only the data for $[W]_0 = 3.45$ mass%). The agreement between simulation results and industrial data is observed to be quite good. The values of μ_n at $\tau = 1$ for these two runs are given in *Table 8*. These are in good agreement and are shown in *Figure 13*. The agreement between model results using parameters 'tuned' only on one set of data ($[W]_0 = 3.45\%$) and industrial data at two other values of $[W]_0$ lends credence to the model. It may be added that the agreement between the model results and industrial data, as obtained in this study, is slightly better than that observed in our previous study[6]. The present model, however, offers advantages, as discussed earlier, and is more suited for optimization work.

We next explored whether we could improve the agreement between the predicted values of $\theta(\tau)$ in regions

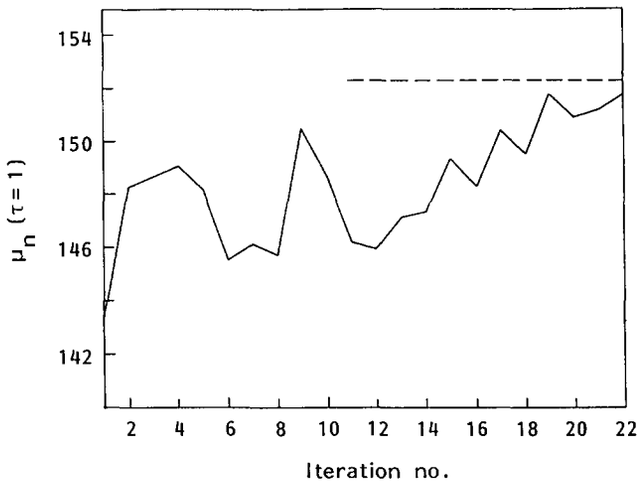

Figure 8 Variation of μ_n ($\tau = 1$) with iteration number for the case shown in *Figure 6*: ---, experimental value of μ_n

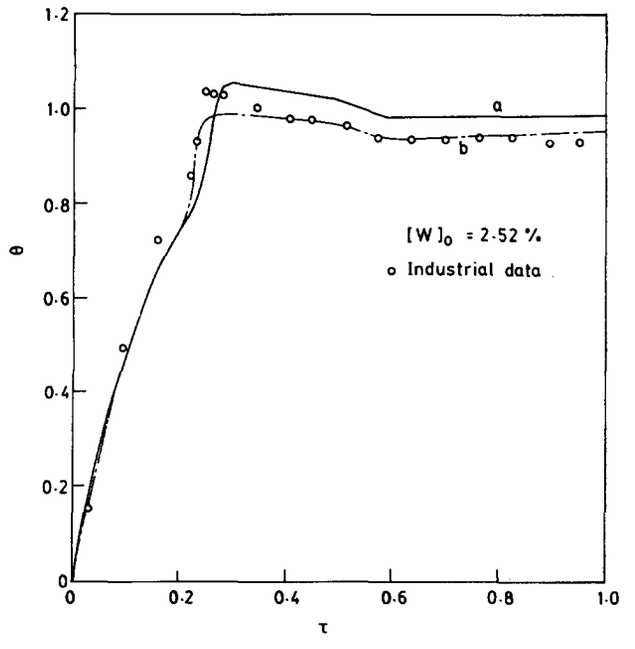

Figure 9 Variation of the dimensionless temperature, θ, with dimensionless time, τ, for $[W]_0 = 2.52$ mass%. Parameters of *Table 5* used to generate simulation results (curves) for cases a and b. ○, Industrial data

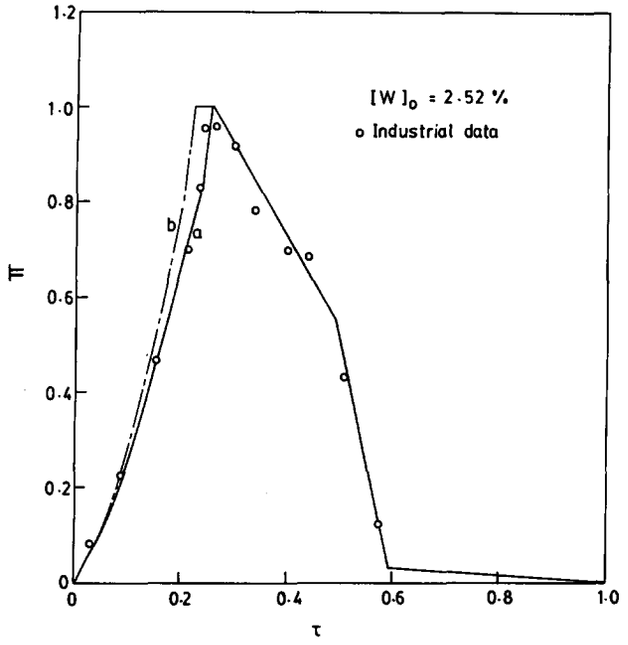

Figure 10 Variation of the dimensionless pressure, Π, with dimensionless time, τ, for $[W]_0 = 2.52$ mass%. Notation as in *Figure 9*

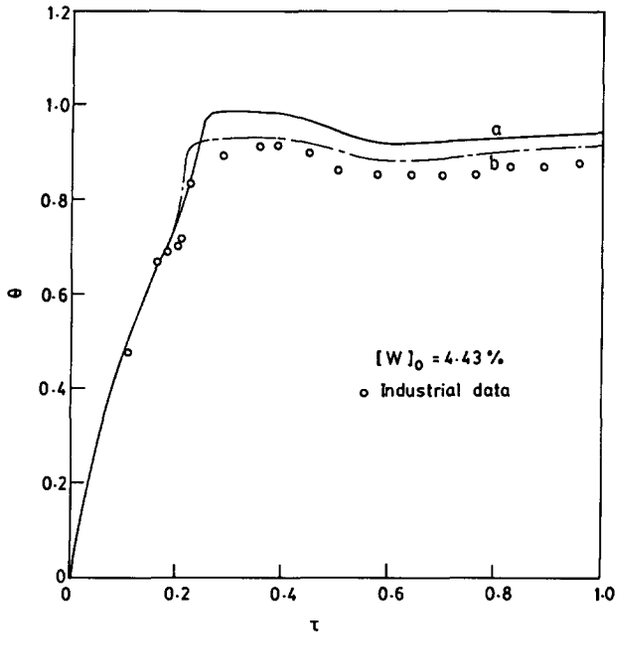

Figure 11 Variation of the dimensionless temperature, θ, with dimensionless time, τ, for $[W]_0 = 4.43$ mass%. Notation as in *Figure 9*

3–5 and the industrial points, without worsening the agreements in Π(τ) in region 1 and $\mu_n(\tau = 1)$. This could be achieved only by changing some of the parameters other than ***p*** in *Table 5*, case a, and correlations used in our model, e.g. those given in *Tables 2* and *4*. These correlations and parameters were compiled from the literature and were used to generate *Figures 4–13* (case a) without change, even though some disagreements and questions on their applicability to nylon 6 systems have been reported. For example, Tai *et al.*[8] have reported variations of the parameters in *Table 2* characterizing the rate and equilibrium constants, as the initial water

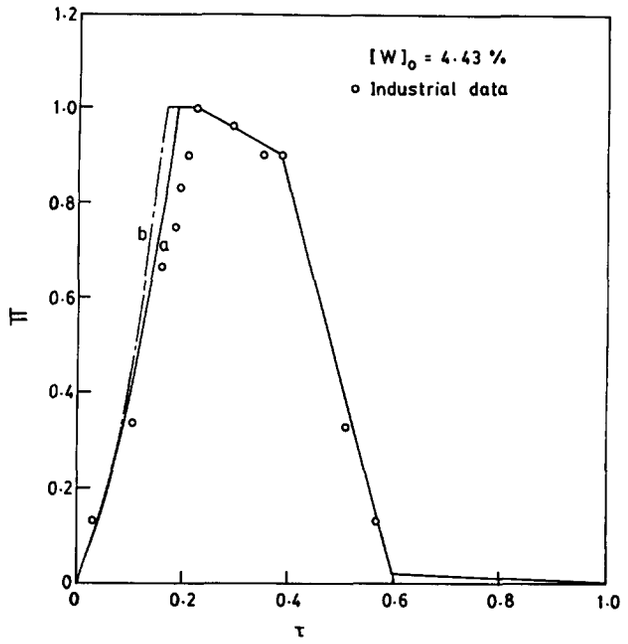

Figure 12 Variation of the dimensionless pressure, Π, with dimensionless time, τ, for $[W]_0 = 4.43$ mass%. Notation as in *Figure 9*

Table 8 Number average chain lengths of product under different conditions

	$\mu_n(\tau = 1)$		
$[W]_0$ (mass%)	Industrial	Computed (case a)	Computed (case b)
2.52	156.0	155.53	155.997
3.45	152.5	151.76	152.234
4.43	150.625	150.62	150.146

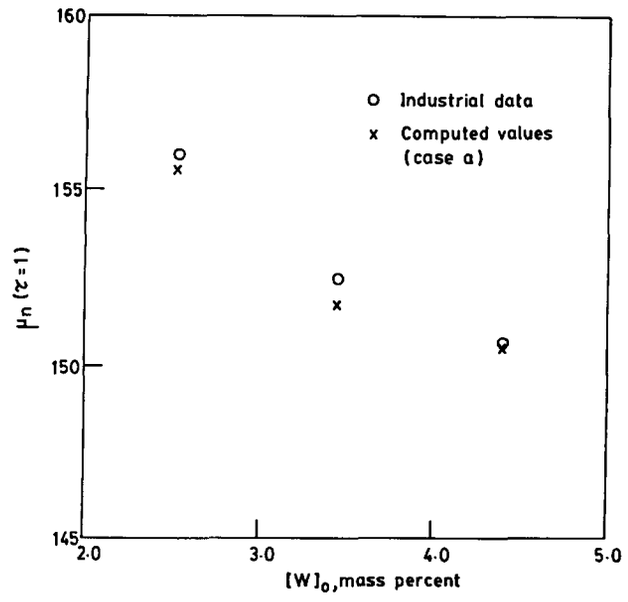

Figure 13 Computed (case a) and industrial values of μ_n $(\tau = 1)$ for the three feed-water concentrations

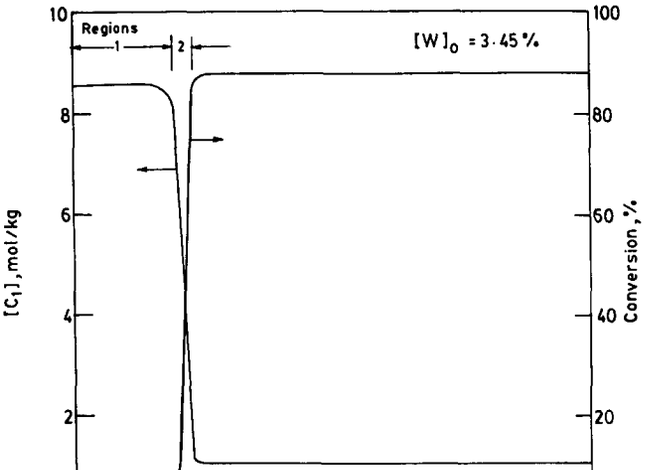

Figure 14 Model results for $[C_1](\tau)$ and conversion for $[W]_0 = 3.45\%$ using parameter values of *Table 5*, case b

concentration is changed. Similarly, the parameters used to estimate the mass transfer coefficients have been developed on systems having far lower viscosities than encountered in nylon 6 reactors. A parametric sensitivity study was carried out by varying several parameters (k, D_w, D_m, λ_m, λ_w, $C^v_{p,m}$, $C^v_{p,w}$, ΔH_1, ΔH_2, ΔH_3, A^c_2, R_{vm}, R_{vw}, $\boldsymbol{p}$) one at a time around their reference values (by about $\pm 30\%$), and observing the effect on $\theta(\tau)$, $\Pi(\tau)$ and $\mu_n(\tau = 1)$. The results are summarized below:

(a) only h_{ref} significantly influences $\theta(\tau)$ in region 1;
(b) the value of $\mu_n(\tau = 1)$ is affected only by ΔH_2, ΔH_3 and β_{wf};
(c) only β_{wo} affects $\Pi(\tau)$ in region 1.

Other than these, there were insignificant changes.

We also evaluated the importance of the different individual terms in the energy balance equation (dT/dt in *Table 3*) at different values of τ, using the reference values of the parameters (those in *Tables 2* and *4*, and *Table 5*, case a). We made the following observations (see *Figure 4*).

(a) Heat transfer from the jacket fluid dominates in the beginning until $\tau \approx 0.2$. The value of h_{ref} used is important in this zone.
(b) A considerable amount of heat is generated by the polyaddition reaction, i.e. the term involving $(-\Delta H_3)r_3$, around $\tau \approx 0.2$. This leads to a very sudden increase in θ from about 0.8 to 1.05. Reduction of the parameters associated with r_3, or of the value of $(-\Delta H_3)$ could lead to a lowering of the maximum value of $\theta(\tau)$.
(c) The value of dT/dt is much smaller after the peak in $\theta(\tau)$. Thus, the lowering of $\theta_{max}(\tau)$ achieved by a reduction in $r_3(-\Delta H_3)$ could persist until later times, and improve the fit between model results and industrial data.

In view of these observations, it was decided to try out lower values of E^c_3 and $(-\Delta H_3)$, two of the parameters which influence the $r_3(-\Delta H_3)$ term in the energy balance equation. Use of $E^c_3 = 0.9\ E^c_{3,ref}$ and $(-\Delta H_3) = 0.9 \times (-\Delta H_3)_{ref}$ led to fairly good agreement in $\theta(\tau)$ but worsened the fit between predicted and observed values of $\Pi(\tau)$ and of $\mu_n(\tau = 1)$. These effects could be compensated for by retuning the values of $\boldsymbol{p}$. The Box complex method was tried again for the $[W]_0 = 3.45\%$ case, and the best fit values of the new parameters are given in *Table 5* (case b). All other values are as given in *Tables 2* and *4*. The agreement between model results and industrial data for the $[W]_0 = 3.45\%$ run is seen from *Figures 4* and *5* (case b) to be much better than for case a. These values are then used to predict (without further tuning) the results for the other two values of $[W]_0$. *Figures 9–12* (case b) show the agreement to be fairly good. The corresponding values of $\mu_n(\tau = 1)$ for case b are given in *Table 7*, and these agree well with the industrial values.

A justification for the use of modified values of E^c_3 and $(-\Delta H_3)$ for case b is called for at this stage. The reference values of these parameters used in case a are average values suggested by Tai *et al.*[8]. However, E^c_3 has been reported to vary from 8.374×10^4 to 8.4407×10^4 J mol^{-1}, and ΔH_3 from -1.6734×10^4 to -1.7595×10^4 J mol^{-1}. Thus, we see that there is indeed some amount of flexibility available in the choice of these two parameters, though not as much as 10% used in case b. The availability of more industrial data (e.g. variation of μ_n with τ, vapour concentrations or condensate analysis as a function of time, etc.) would definitely help in resolving whether some other parameters could be changed as well, keeping values of E^c_3 and ΔH_3 within the ranges suggested by Tai *et al.*[8]. Until such data become available, we are almost compelled to accept the values of E^c_3 and ΔH_3 as given in *Table 5* (case b) as curve-fit values for the particular reactor we are simulating. It is hoped that this simulation study will generate interest among researchers able to provide more industrial data, in order to resolve some of these issues.

Finally, we give some additional interesting simulation results using the parameter values for case b. *Figure 14* shows how the monomer concentration decreases sharply at about $\tau \approx 0.2$ to almost its final value for $[W]_0 = 3.45\%$. The sharp decrease in $[C_1]$ occurs during region 2. The monomer conversion is also plotted in this diagram. The results for the other two values of $[W]_0$ are almost indistinguishable and so are not plotted. *Figure 15* shows how μ_n increases in two stages to its final value for all three feed-water concentrations. The initial (up to $\tau \approx 0.2$) sharp rise in μ_n is associated with the polyaddition reaction (note that this is associated with almost the entire consumption of the monomer, see *Figure 14*), while the later increase in μ_n ($\tau > 0.5$) is associated with the polycondensation reaction (with little change in the monomer concentration). The polydispersity index (*PDI*) attains a value of 2.0 for $\tau \gtrsim 0.24$. *Figure 16* shows the gradual build-up of the cyclic dimer concentration for the three feed-water concentrations. It may be pointed out that *Figures 15* and *16* show the compounded effects of changing $[W]_0$ as well as the pressure history. It is interesting that the final monomer conversion is relatively insensitive to these two operating parameters. This point has interesting ramifications for optimization studies.

Figure 17 shows how R_{vm}, R_{vw} and V_T vary with time for the $[W]_0 = 3.45\%$ case. All these three variables show local maxima in two regions, the first near $\tau \approx 0.2$ when the control valve opens for the first time (region 2), and the second during $0.4 < \tau < 0.6$ (region 4). The latter is associated with a relatively sharp decrease in Π. It is

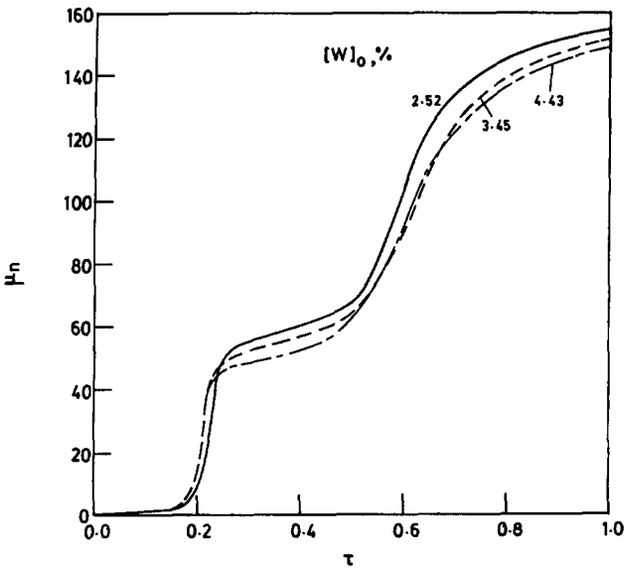

Figure 15 Model results for $\mu_n(\tau)$ for three feed-water concentrations ($[W]_0$ (mass%): ——, 2.52; – – –, 3.45; — — —, 4.43) using parameter values of *Table 5*, case b

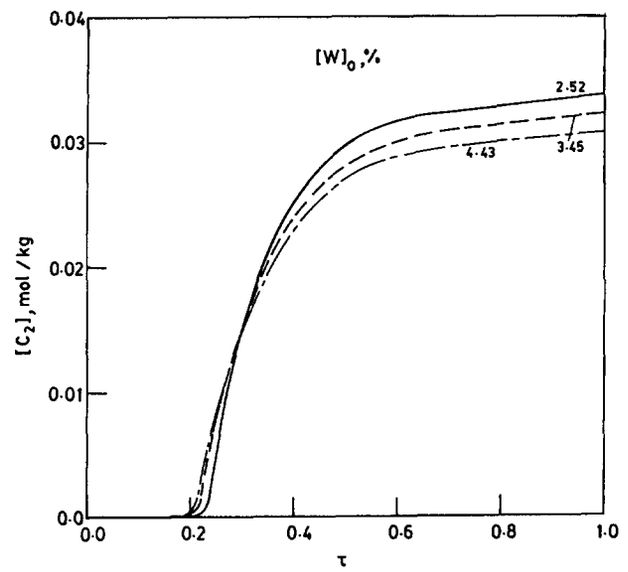

Figure 16 $[C_2](\tau)$ for three feed-water concentrations. Notation as in *Figure 15*

interesting to mention that the concentration of the inert falls sharply to negligible values after $\tau \approx 0.2$. By this time, the vapour space has a preponderance of H_2O. In fact, the $[W^v](\tau)$ history looks quite similar to the $\Pi(\tau)$ history. The sharp changes in R_{vw} with time lead to numerical problems in the integration of the corresponding adjoint variables in our optimization studies.

Figure 18 shows how the viscosity (η) and Reynolds number (N_{Re}) vary with time for $[W]_0 = 3.45\%$. At the beginning, η decreases with time owing to the increase in temperature. Thereafter, it increases by three orders of magnitude over a relatively short time-span. This is associated with the increase in molecular weight as well as concentration of the polymer near $\tau \approx 0.2$. There is a second period of increase of η, associated with a similar second phase of increase in μ_n (or μ_w), as shown in *Figure 15*. The Reynolds number follows the reverse trend.

Figure 19 shows that the overall heat transfer coefficient, U, follows a trend similar to that shown by $N_{Re}(\tau)$. However, the change of U, for $0.4 < \tau < 0.6$, is much smaller. It is interesting to note that U is almost constant after $\tau \approx 0.2$. This fact can be used to simplify the equations for the adjoint variables in optimization studies. *Figure 20* suggests that similar simplifications (of constant coefficients for $\tau > 0.2$) cannot be made for the three mass transfer coefficients.

CONCLUSIONS

A systematic simulation of an industrial semibatch nylon 6 polymerization reactor is made taking into consideration the vaporization of water and monomer. A very general computer package was prepared to solve the set of differential equations obtained from the mass and energy balance equations. The main differences from our earlier studies on this reactor are in the energy balance

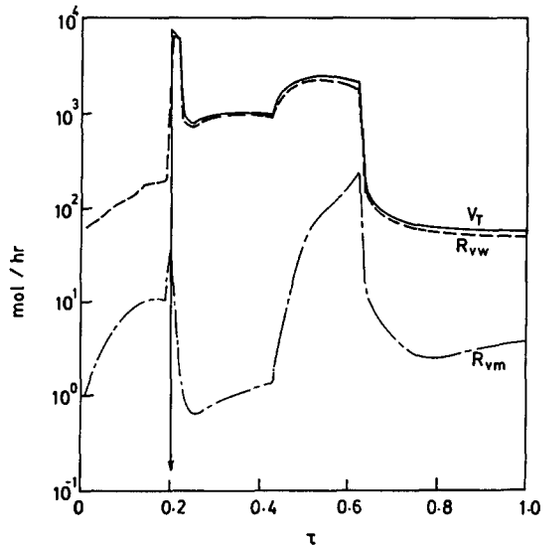

Figure 17 R_{vm}, R_{vw} and V_T as a function of τ for $[W]_0 = 3.45\%$, using parameter values of *Table 5*, case b. $V_T = 0$ for $\tau < 0.2$

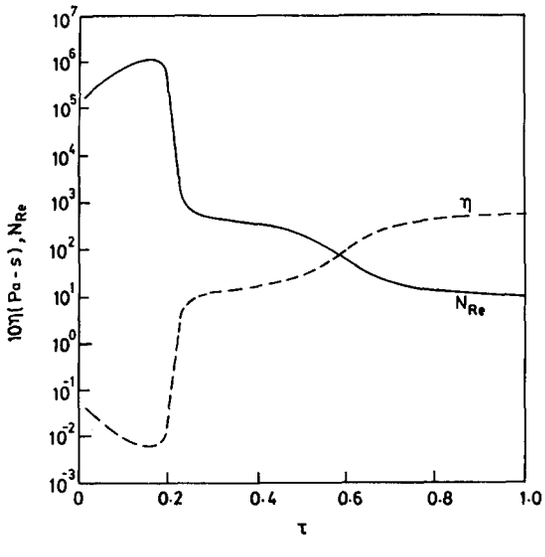

Figure 18 Variation of viscosity (η) and Reynolds number (N_{Re}) for $[W]_0 = 3.45\%$, using parameter values of *Table 5*, case b

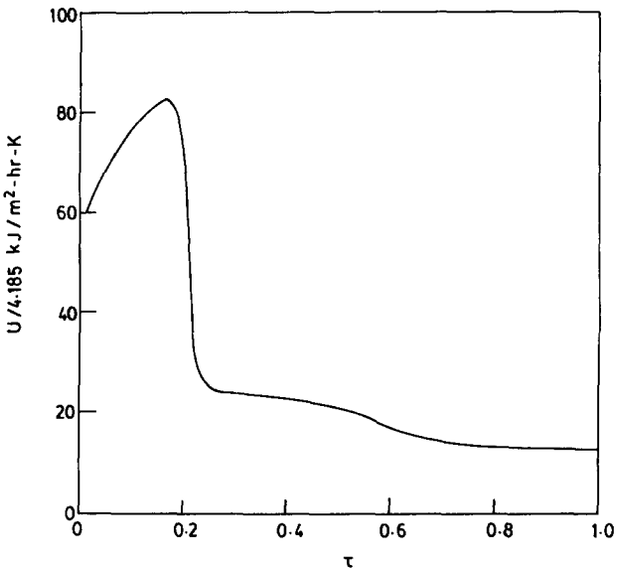

Figure 19 Variation of the overall heat transfer coefficient with time for $[W]_0 = 3.45\%$, using parameter values of *Table 5*, case b

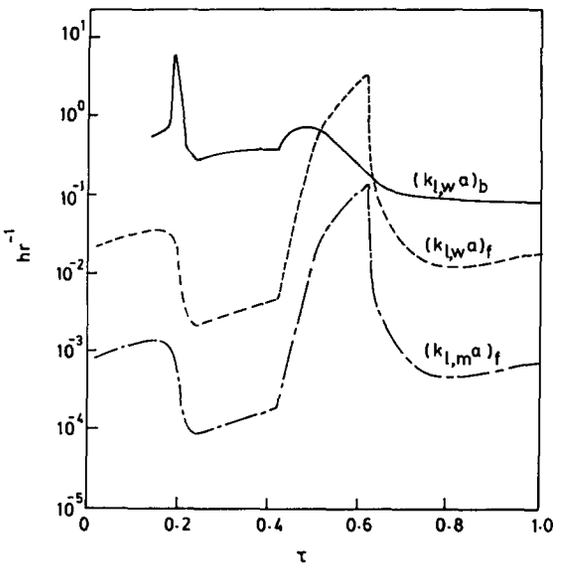

Figure 20 Variation of the three mass transfer coefficients with time for $[W]_0 = 3.45\%$ using parameter values of *Table 5*, case b

equation and in the equations for the activity coefficients, which are now written in terms of monomer conversion. Discontinuities in γ_m and γ_w are thereby avoided. A set of five curve-fit parameters (in the equations for the activity coefficients and the heat transfer coefficient) are obtained for one feed-water concentration. These predict fairly well the behaviour at two other feed-water concentrations, thus justifying the use of the model. Some interesting simplifications have been suggested which can be used in future optimization studies on this reactor.

REFERENCES

1 Reimschuessel, H. K. *J. Polym. Sci., Macromol. Rev.* 1977, **12**, 65
2 Tai, K. and Tagawa, T. *Ind. Eng. Chem., Prod. Res. Dev.* 1983, **22**, 192
3 Gupta, S. K. and Kumar, A. *J. Macromol. Sci., Rev. Macromol. Chem. Phys.* 1986, **C26**, 183
4 Gupta, S. K. and Kumar, A. 'Reaction Engineering of Step Growth Polymerization', Plenum, New York, 1987
5 Gupta, A , Gupta, S. K., Gandhi, K. S., Ankleshwaria, B. V., Mehta, M. H., Padh, M. R. and Soni, A. V. in 'Recent Trends in Chemical Reaction Engineering' (Eds B. D. Kulkarni, R. A. Mashelkar and M. M. Sharma), Wiley, New Delhi, 1987, pp. 281–297
6 Gupta, A., Gupta, S. K., Gandhi, K. S., Mehta, M. H., Padh, M. R., Soni, A. V. and Ankleshwaria, B. V. *Chem. Eng. Commun.* 1992, **113**, 63
7 Tai, K., Teranishi, H., Arai, Y. and Tagawa, T. *J. Appl. Polym. Sci.* 1979, **24**, 211
8 Tai, K., Teranishi, H., Arai, Y. and Tagawa, T. *J. Appl. Polym. Sci.* 1980, **25**, 77
9 Arai, Y., Tai, K., Teranishi, H. and Tagawa, T. *Polymer* 1981, **22**, 273
10 Tai, K., Arai, Y., Teranishi, H. and Tagawa, T. *J. Appl. Polym. Sci.* 1980, **25**, 1789
11 Tai, K., Arai, Y., Teranishi, H. and Tagawa, T. *J. Appl. Polym. Sci.* 1982, **27**, 731
12 Tai, K. and Tagawa, T. *J. Appl. Polym. Sci.* 1982, **27**, 2791
13 Giori, C. and Hayes, B. T. *J. Polym. Sci. A1* 1970, **8**, 335
14 Giori, C. and Hayes, B. T. *J. Polym. Sci. A1* 1970, **8**, 351
15 Gupta, A., PhD Thesis, Indian Institute of Technology, Kanpur, 1987
16 Snell, F. D. and Ettre, L. S. 'Encyclopedia of Industrial Chemical Analysis', Vol. 8, Interscience, New York, 1969
17 Reid, R. C., Prausnitz, J. M. and Poling, B. E. 'The Properties of Gases and Liquids', 4th edn, McGraw Hill, New York, 1988
18 Kirk, R. E. and Othmer, D. F. 'Encyclopedia of Chemical Technology', Vol. 18, 3rd edn, Wiley, New York, 1982, p. 328
19 Tai, K., Arai, Y. and Tagawa, T. *J. Appl. Polym. Sci.* 1983, **28**, 2527
20 Hikita, H. and Konishi, Y. *AIChE J.* 1984, **10**, 945
21 Ray, A. K. and Gupta, S. K. *J. Appl. Polym. Sci.* 1985, **30**, 4529
22 Pal, D. and Gupta, S. K. *Polymer* 1989, **30**, 1918
23 Box, M. *Computer J.* 1965, **8**, 42
24 Kuester, J. L. and Maize, J. H. 'Optimization Techniques with Fortran', McGraw Hill, New York, 1973
25 Kumar, V. R. and Gupta, S. K. *Polymer* 1991, **32**, 3233

NOMENCLATURE

a	Specific interfacial area ($m^2\ m^{-3}$)
A	Jacket area (m^2)
A_i	Frequency factor for ith reaction rate constant ($kg\ mol^{-1}\ h^{-1}$)
c, C_s'	Concentration of polymer in solution ($kg/100\ kg$, $g\ cm^{-3}$)
$[C_i]$	Concentration of caprolactam (1) and cyclic dimer (2) in liquid phase (mol/kg mixture)
$C_{p,i}^v$	Specific heat of pure i in vapour phase ($kJ\ kg^{-1}\ K^{-1}$)
$C_{p,mix}^l$	Specific heat of liquid reaction mixture ($kJ\ kg^{-1}\ K^{-1}$)
d_s	Diameter of stirrer (m)
$\mathscr{D}_i$	Diffusivity of component i ($m^2\ h^{-1}$)
D_r	Diameter of reactor (m)
D_w	Reactor wall thickness (m)
DP	Degree of polymerization of polymer product
E_i	Activation energy of ith reaction ($J\ mol^{-1}$)
F	Mass of liquid in reactor at time t (kg)
h_i	Heat transfer coefficient of liquid ($kJ\ m^{-2}\ h^{-1}\ K^{-1}$)
ΔH_i	Enthalpy change for ith reaction ($J\ mol^{-1}$)
k	Thermal conductivity of reaction mass ($kJ\ m^{-1}\ h^{-1}\ K^{-1}$)
k_i	Rate constant for ith reaction ($kg\ mol^{-1}\ h^{-1}$)
$k_{l,i}$	Mass transfer coefficient of component i ($m\ h^{-1}$)
K_i	Equilibrium constants for ith reaction
$[M^v]$	Concentration of caprolactam in vapour phase ($mol\ m^{-3}$)
M_n	Number average molecular weight

M_w	Weight average molecular weight
n	Rate of rotation of stirrer (rev min^{-1})
$[N^v]$	Concentration of nitrogen in vapour phase (mol m^{-3})
N_{Re}	Reynolds number
N_{Sc}	Schmidt number
N_{Sh}	Sherwood number
P	Total pressure (kPa)
P_i^{sat}	Vapour pressure of component i (kPa)
Q	Polydispersity index
r_i	Net forward rate for ith reaction (mol kg^{-1} h^{-1})
R	Universal gas constant (kPa m^3 mol^{-1} K^{-1} or J mol^{-1} K^{-1})
R_{vm}	Rate of evaporation of caprolactam (mol h^{-1})
R_{vw}	Rate of evaporation of water (mol h^{-1})
$[S_i]$	Concentration of linear oligomers in liquid (mol kg^{-1})
ΔS_i	Entropy change for ith reaction (J mol^{-1} K^{-1})
t	Time (h)
t_f	Total reaction time (h)
T	Temperature (K)
T_r	Reference temperature (=473.15 K)
U	Overall heat transfer coefficient (kJ h^{-1} m^{-2} K^{-1})
V_g	Volume of vapour space (m^3)
V_T	Rate of vapour escape from reactor (mol h^{-1})
[W]	Water concentration in liquid (mol/kg mixture)
$[W^v]$	Concentration of water in vapour (mol m^{-3})
x_i	Mole fraction of ith species
γ_i	Activity coefficient of i
η	Viscosity of liquid mixture (Pa s or poise; 1 poise = 10^{-1} Pa s)
$[\eta]$	Intrinsic viscosity of ε-caprolactam–nylon 6 mixture (100 kg mixture/kg polymer)
ζ_i	Total mol of m ($i=1$), w ($i=2$) or both ($i=3$) vaporized to time t (mol)
θ	Dimensionless temperature (equation (10))
λ_i	Latent heat of vaporization of i (kJ mol^{-1})
μ_i	Moments of the S_n distribution
μ_n	Number average chain length ($\equiv \mu_1/\mu_0$)
Π	Dimensionless pressure (equation (10))
ρ	Density of liquid mixture (kg m^{-3})
τ	Dimensionless time (equation (11))

Subscripts/superscripts

b	Bubble
expt	Experimental value
f	Free surface
j	Jacket
l	Liquid
m	Monomer
o	Feed conditions
theor	Theoretical value (using model)
v	Vapour
w	Water